Degenerate Four-Wave Mixing Measurements of High Order Nonlinearities in Semiconductors

E. J. Canto-Said, D. J. Hagan, *Member, IEEE*, J. Young, and Eric W. Van Stryland, *Senior Member, IEEE*

Abstract—**We describe degenerate four-wave mixing experiments on ZnSe and CdTe semiconductor samples with picosecond laser pulses at wavelengths below the bandgap. Nonlinearities of third, fifth, and seventh order are observed and the mechanisms for each are identified. In all of our measurements, we observe a fast third order nonlinearity. For two-photon absorbers, this is attributed to contributions from both the real (refractive) and imaginary (absorptive) parts of the third-order susceptibility. Below the two-photon absorption edge, the nonlinearity is purely refractive. The higher order effects are due to carriers generated by multiphoton excitation. In ZnSe at 0.532 μm, carriers are generated by two-photon absorption such that a fifth order nonlinearity arises from the change in index due to these carriers, a sequential $\chi^{(3)}:\chi^{(1)}$ nonlinearity. From such measurements we determine the refractive index change per photoexcited carrier pair and the density dependence of the carrier diffusion coefficient. Analogous signals are observed in CdTe at 1.064 μm. The seventh order nonlinearity observed in ZnSe at 1.064 μm results from the refractive index contribution of carriers generated by three-photon absorption.**

I. Introduction

We report a series of picosecond degenerate four-wave mixing (DFWM) studies conducted in ZnSe and CdTe at wavelengths of 0.532 and 1.064 μm. The DFWM signal shows a fast third order nonlinearity, as well as higher order slowly decaying nonlinearities due to multiphoton absorption generated carriers. We attribute this signal to the combined effects of the real and imaginary parts of the third order susceptibility $\chi^{(3)}$. The imaginary part corresponds to two-photon absorption (2PA), while the real part is due to bound-electronic nonlinear refraction (index n_2), as opposed to a free-carrier effect [1]. From our measurements, we obtain the absolute value of the third order nonlinear susceptibility for both ZnSe and CdTe. This, combined with independent 2PA measurements, allows us to extract the real part of the susceptibility which corresponds to the nonlinear refraction.

We also observe a rapid third order nonlinear effect which is dominant at low incident irradiances in both semiconductors when all three beams are temporally coincident (zero delay). Fifth and seventh order nonlinear effects are evident, depending on wavelength, when the gratings are probed at time delays greater than the pulsewidth to eliminate the signal from the fast third order effect. These higher order refractive nonlinearities are attributed to the refractive effect of carriers generated by 2PA (fifth order) and 3PA (seventh order). Most of the experiments discussed here consist of the generation of a modulated carrier density or carrier grating created by interfering two of the three beams made coincident in the semiconductor sample. Diffraction of a third beam from this grating produces a DFWM signal yielding information on the nonlinearities resulting from the photogenerated carriers and their decay mechanisms [2], [3]. Decay of this signal, which is the phase conjugate of one of the two interfering beams, takes place due to carrier diffusion and recombination. An expression for the diffraction efficiency at long temporal delays is obtained from coupled-wave theory [4]. This expression leads to a calculation of the index of refraction change per carrier pair per unit volume generated via 2PA in ZnSe at 0.532 μm. Measurements of the grating decay for several pump-probe angles gives values for the carrier diffusion and recombination lifetimes in ZnSe at 0.532 μm.

After describing the experimental techniques in Section II, we identify in Section III-A the dominant nonlinearities in the two materials ZnSe and CdTe. We determine these to be fast third order nonlinearities, due to the same processes which give rise to the effects of bound-electronic refraction and two-photon absorption, while higher order effects are due to free-carrier refraction. In Section III-B we describe our measurements of the absolute magnitude of the combined third order susceptibilities. Studies of higher order effects due to free-carrier gratings are discussed in Section III-C. In order to obtain a quantitative measurement of the carrier induced nonlinearities, in Section III-D we develop an expression for the diffraction efficiency of these carrier gratings and hence find a value for the free-carrier refractive index coefficient in ZnSe. By measuring the angular dependence of the grating decay, we determine the carrier diffusion coefficient as a function of carrier density.

Manuscript received December 28, 1990; revised May 1, 1991. This work was supported in part by the National Science Foundation by Grant ECS#8617066, DARPA/CNVEO, and the Florida High Technology and Industry Council.

E. J. Canto-Said is with McLennan Physical Laboratories, The University of Toronto, Toronto, Ont., Canada M5S 1A7.

D. J. Hagan is with the Department of Physics, Center for Research in Electro-Optics and Lasers (CREOL), University of Central Florida, Orlando, FL 32816.

J. Young is with the Department of Physics, Heriot Watt University, Edinburgh EH14 4AS, Scotland.

E. W. Van Stryland is with the Departments of Physics and Electrical Engineering, Center for Research in Electro-Optics and Lasers (CREOL), University of Central Florida, Orlando, FL 32816.

IEEE Log Number 9101808.

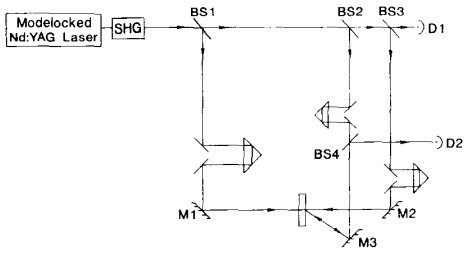

Fig. 1. Schematic of experimental DFWM apparatus. D_1 is the input pulse energy monitor, while D_2 monitors the phase-conjugate signal pulse energy.

II. Experimental Technique

In our experiments the "backward" DFWM geometry is used. A schematic of the experimental geometry using single 43 ps (FWHM) 1.064 μm pulses, or 30 ps (FWHM) 0.532 μm pulses is shown in Fig. 1. The picosecond, Gaussian spatial profile pulses are derived from a Q-switched mode-locked Nd:YAG laser system operating at 1.064 μm. An electrooptic switch between the oscillator and amplifier ensures single pulse performance. A second-harmonic crystal (KDP) produces the 0.532 μm pulses. This single pulse is divided into three pulses which, after passing through variable time delays, are incident on the semiconductor samples. The three pulses can be independently adjusted in amplitude and polarization using half-wave plate and polarizer combinations. Two strong beams, forward (E_f) and backward (E_b) pumps, of approximately equal irradiance are incident on the semiconductor from counterpropagating directions. A weaker beam, the probe (E_p), is incident on the sample at an angle θ with respect to E_f. The grating spacing determined from the angle θ can be varied from 1.2 to 8 μm for the experiments at 0.532 μm. At 1.064 μm the grating spacing is fixed at 8 μm. The conjugate wave E_c, which retraces the path of E_p, is detected by a large area integrating photodiode as are various reference beams. These detectors are calibrated against pyroelectric energy monitors. All pulsewidths quoted are measured by autocorrelation using a second-harmonic generator, while all quoted spot sizes were measured in both horizontal and vertical directions at the sample position by the method of scanning pinholes.

The samples used in this series of experiments consist of zincblende, chemical-vapor-deposition-grown polycrystalline samples of ZnSe and CdTe [5]. The ZnSe sample was 3 mm thick and the CdTe was 2 mm thick.

III. Results and Discussion

A. Identification of the Nonlinear Processes

Using pulses at 0.532 μm, the DFWM signal in ZnSe was monitored as a function of input energy and pulse delay for different combinations of the polarization of the three input beams. Fig. 2 shows a plot of the signal versus the delay τ_b of E_b, with E_b polarized perpendicular to both E_f and E_p. The angle θ between the forward pump and probe, measured outside the sample, was 13° and the peak input irradiance of each pump was $I_b \simeq 34$ MW/cm^2 and $I_f \simeq 22$ MW/cm^2. Clearly, two very distinct nonlinearities are evident from Fig. 2. Near zero delay, a large rapidly decaying signal is seen, while at longer delays, we observe a more slowly decaying signal. To better understand the two nonlinear regimes, irradiance dependence experiments were performed at different delays. Fig. 3 shows a log–log plot of the DFWM signal versus the total input irradiance, (all three input beams were varied simultaneously) at two different delay times. Fig. 3(a) shows the irradiance dependence at zero delay. The least-squares fit gives a power dependence of $I^{3.2\pm0.2}$, indicative of a third order nonlinearity dominant at the zero delay peak. Fig. 3(b) shows the dependence at a delay of 240 ps, with a best fit giving a power dependence of $I^{5.0\pm0.2}$. The fifth order dependence of the DFWM signal on the input beams can be explained by 2PA induced carrier refraction. This mechanism can be viewed as a two step process. First, a modulated carrier density is generated via 2PA; this is an Im $\{\chi^{(3)}\}$ effect. Second, a third beam diffracts off the carrier modulation; this is a Re $\{\chi^{(1)}\}$ effect. Hence, the mechanism is a sequential $\chi^{(3)}:\chi^{(1)}$ process that appears as an overall fifth order nonlinearity [6]. Studies in CdTe at 1.06 μm, where this material exhibits 2PA, reveal the same basic behavior, i.e., a fast third order signal followed by a slowly decaying fifth order signal.

B. Fast Third Order Nonlinearity

The third order effect observed near zero delay, as can be seen from Fig. 2, decays within the 30 ps pulsewidth, and appears unchanged when the pump-probe angle is varied. As DFWM is sensitive only to the absolute value of $\chi^{(3)}$, this third order signal may arise from both the real and imaginary parts of the susceptibility, $\chi_R^{(3)}$ and $\chi_I^{(3)}$, where $\chi^{(3)} = \chi_R^{(3)} + i\chi_I^{(3)}$. We define $\chi^{(3)}$ in terms of the nonlinear polarization in c.g.s.-Gaussian units by: $\boldsymbol{P} = \chi^{(1)}\boldsymbol{E} + \chi^{(3)}|\boldsymbol{E}|^2\boldsymbol{E}/2$. For all beams linearly polarized parallel to each other, $\chi^{(3)} = 6\chi^{(3)}_{1111}$[11], as we are dealing with polycrystalline (grain size $\simeq 1$ μm) and hence effectively isotropic media. The source of $\chi_I^{(3)}$ in the range $E_g/2 \le \hbar\omega \le E_g$, is 2PA (coefficient β_2). The real part of $\chi^{(3)}$ corresponds to nonlinear refraction. Usually, this nonlinear refraction is expressed in terms of n_2, where $n_2 = n_0 + n_2|E|^2/2$. n_2 and β_2 are related to $\chi^{(3)}$ by

$$n_2 = \frac{2\pi}{n_0}\chi_R^{(3)} \tag{1}$$

and

$$\beta_2 = \frac{4\pi\omega}{9\times10^8\,\epsilon_0 n_0^2 c^2}\chi_I^{(3)} \tag{2}$$

where ϵ_0 is the permittivity of free space, n_0 is the linear refractive index, and c is the speed of light in vacuum. Here n_2 and $\chi^{(3)}$ are expressed in esu, and all other parameters are in MKS units. We can estimate the magnitude of n_2 from measurements of the DFWM reflectivity ϵ_c/ϵ_p,

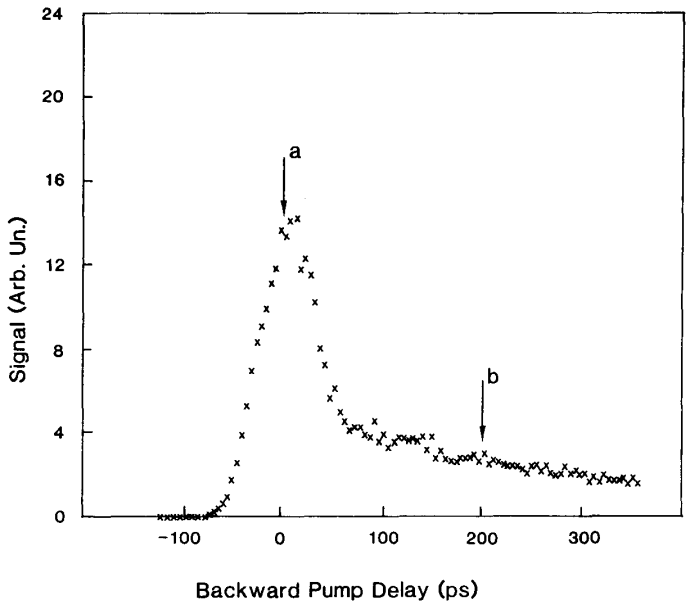

Fig. 2. Phase-conjugate signal versus backward pump delay for a 13° pump–probe angle and with the backward pump polarized perpendicular to the other two waves. The peak pump irradiances are $I_f = 22$ MW/cm^2 and $I_b = 34$ MW/cm^2.

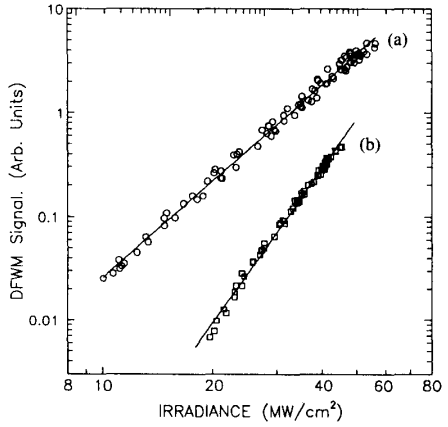

Fig. 3. Log–log plots of the phase conjugate signal versus the total input irradiance ($I_f + I_b + I_p$) as all three beams were varied together, for (a) zero delay and (b) 240 ps delay. The solid lines are best fits to the data giving power dependencies of $I^{3.1\pm0.2}$ and $I^{5.0\pm0.2}$, respectively. The other experimental parameters are as in Fig. 2.

where ϵ_c and ϵ_p are the energies of the conjugate and probe pulses, respectively. In the degenerate case for small reflectivity and in the "undepleted" pumps approximation the third order susceptibility is given by [7]

$$|\chi^{(3)}|^2 = \frac{n^4 c^4 \epsilon_0^2}{\omega^2 L^2 I_f I_b} \frac{I_c}{I_p} \tag{3}$$

where I is the peak irradiance for each beam, n is the linear refractive index, and L is the sample thickness. In (3), the ratio of irradiances is given by

$$I_c/I_p = \frac{\epsilon_c}{\epsilon_p} \frac{t_p}{t_c} \left(\frac{w_p}{w_c}\right)^2. \tag{4}$$

For ZnSe $n = 2.7$ [9], $L = 0.3$ cm, and the measured probe and calculated conjugate spot radii are $w_p = 1.41$ mm (HW1/e^{2}M) and $w_c = 0.99$ mm, respectively. t_p/t_c is the ratio of the probe to conjugate beam pulsewidth which for a third order effect should equal $\sqrt{3}$, giving $I_c/I_p = 0.069$. At zero delay and 0.532 μm the DFWM energy reflectivity of ZnSe was measured to be 1.6% for $I_f = 46$ MW/cm^2, $I_b = 65$ MW/cm^2, and $I_p \simeq I_f/10$. The 2PA coefficient for ZnSe at this wavelength is $\beta_2 \simeq 5.5$ cm/GW, [10] hence at these irradiance levels losses due to 2PA are less than 6%, so that the undepleted pumps approximation is valid. This gives for ZnSe:

$$|\chi^{(3)}| = 2.6 \times 10^{-19} \text{ m}^2/V^2 = 1.9 \times 10^{-12} \text{ esu}$$

where the estimated total absolute error in our measurement is estimated to be $\pm 30\%$. Substituting β_2 in (2) gives $\chi_I^{(3)} = 6.4 \times 10^{-12}$ esu. As this is much smaller than our measured value, this indicates that there must also be a significant real component to $\chi^{(3)}$. Using

$$|\chi^{(3)}| = \sqrt{\left(\chi_R^{(3)}\right)^2 + \left(\chi_I^{(3)}\right)^2}$$

we obtain $|\chi_R^{(3)}| = 1.8 \times 10^{-12}$ esu. Thus, the effect of the 2PA contribution to the DFWM signal is negligibly small, given our estimated errors of $\pm 30\%$. Expressing the measured $|\chi_R^{(3)}|$ in terms of n_2 as $|n_2| = 4.2 \times 10^{-11}$ esu, we find this is in close agreement with the results of

references [1], [8] who measured $n_2 = -4.4 \times 10^{-11}$ esu. using the Z-scan technique.

In order to further investigate the nature of this fast third order susceptibility, we also performed DFWM experiments in polycrystalline CdTe at 1.064 μm. CdTe exhibits 2PA at this wavelength. By measuring the conjugate signal in CdTe versus the delay of the backward pump, using the same configuration as for ZnSe except using 1.064 μm, we see results similar to those shown in Figs. 2 and 3 for ZnSe. At zero delay we find that the signal varies as $I^{3.1\pm0.3}$ while at long delays the signal varies as $I^{4.5\pm0.4}$. For CdTe $\beta \simeq 22$ cm/GW [10] and thus beam depletion due to 2PA is no longer negligible for irradiance levels above $\simeq 50$ MW/cm^2. The somewhat reduced slope observed at long delays can be accounted for by beam depletion at higher irradiances. At an irradiance of $\simeq 35$ MW/cm^2 per pump, the DFWM reflectivity for CdTe is 14.8% at zero delay. This yields a third order susceptibility of $|\chi^{(3)}| = 1.1 \times 10^{-11}$ esu. The 2PA coefficient in CdTe at 1.06 μm has been measured as $\beta_2 = 22$ cm/GW. [10] Hence, $\chi_I^{(3)} = 5.6 \times 10^{-11}$ esu, giving $|\chi_R^{(3)}| = 9.5 \times 10^{-11}$ esu, and $|n_2| = 2.1 \times 10^{-10}$ esu. Once again, this is in remarkably close agreement with Z-scan results, which gave -2×10^{-10} esu [8].

DFWM experiments were also performed in ZnSe at 1.064 μm where it exhibits three-photon absorption. At irradiance levels below 1 GW/cm^2 per pump only a zero delay peak was observed that varied as $I^{2.8\pm0.3}$, indicating the dominance, once again, of a third order nonlinearity. The DFWM signal as a function of delay of the backward pump is shown in Fig. 4, while in Fig. 5 we show a log-log plot of the irradiance dependence of the signal at zero delay. As the phase-conjugate reflectance measured at this wavelength was very much smaller than 4%, the comparative method used previously for determining $\chi^{(3)}$ could not be used in this case. Therefore, $\chi^{(3)}$ was determined by comparison with the known CS_2 value of $n_2 = 1.3 \times 10^{-11}$ esu, and hence $|\chi_{\text{eff}}^{(3)}| = 5.6 \times 10^{-12}$ esu. [12] In order to make such a comparative measurement, we must account for differences in refractive index, surface reflectance and lengths of the two samples by using the following relationship [13]

$$\frac{|\chi_{\text{eff}}^{(3)}(\text{ZnSe})|^2}{|\chi_{\text{eff}}^{(3)}(\text{CS}_2)|^2} = \left[\frac{n_{\text{ZnSe}}}{n_{\text{CS}_2}}\right]^4 \times \text{signal ratio} \times \frac{L_{\text{CS}_2}^2}{L_{\text{ZnSe}}^2} \frac{(1-R)_{\text{CS}_2}^4}{(1-R)_{\text{ZnSe}}^4} \quad (5)$$

where R is the surface reflectance and the signal ratio is the ratio of observed conjugate signal energies for ZnSe and CS_2, respectively. Comparison of the signals from the two materials under identical experimental conditions gives a value of $|\chi^{(3)}| \simeq 1.2 \pm 0.35 \times 10^{-11}$ esu for ZnSe at 1.064 μm. As there is no 2PA in this wavelength region for ZnSe, the imaginary part of $\chi^{(3)}$ is zero. Thus, we can rewrite our result as $|n_2| = 2.7 \pm 0.9 \times 10^{-11}$ esu. This also agrees within errors with Z-scan results, which gave $n_2 = +1.7 \times 10^{-11}$ esu [8].

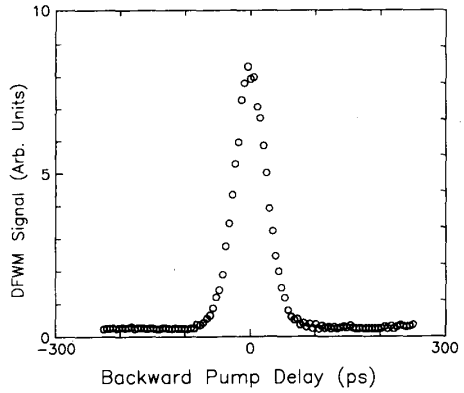

Fig. 4. DFWM signal in ZnSe at 1.064 μm versus backward pump delay with all beams parallel and both pump irradiances $\simeq 600$ MW/cm^2.

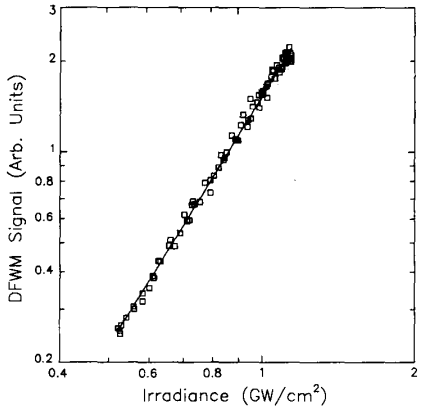

Fig. 5. Logarithmic plot of the DFWM signal in ZnSe at 1.064 μm versus the total incident irradiance, at zero delay. The solid line is a best fit to the data, giving an $I^{2.8\pm0.3}$ dependence.

C. Studies of the Carrier Nonlinearities in ZnSe and CdTe

Neglecting diffusion and recombination within the picosecond pulses, [14] the growth of the carrier density N generated in a 2PA semiconductor is governed by

$$\frac{dN}{dt} = \frac{\beta_2 I^2}{2\hbar\omega} \quad (6)$$

where β_2 is the 2PA coefficient. Here we have ignored the z dependence of N which is valid for our experiments in ZnSe at 0.532 μm where the irradiance is low and, therefore, the 2PA is small ($\leq 6\%$ loss). In the DFWM geometry $I^2 = (E_f + E_b + E_p)^4$. We concentrate only on those terms which contain $E_f E_p^*$ (for the large period grating) and neglect terms in $|E_p|^2 E_p^*$ since $|E_p| \ll |E_f|, |E_b|$. Then the component of I^2 effective in producing a grating leading to the DFWM signal is $I_{\text{eff}}^2 = (n_0 c \epsilon_0/2)^2 (|E_f|^2 +$

$2|E_b|^2)[2E_fE_p^* + \text{c.c.}]$. Note that while I_{eff}^2 is real, it has been broken down into the sum of two complex conjugate terms. The first gives rise to the conjugate signal, the second to a term which radiates with a wave vector of $\boldsymbol{k}_p - 2\boldsymbol{k}_f$, and hence is not phasematched. As both terms are required to form the sinusoidal grating, we must retain both of them to calculate the solution of the diffusion equation; however, the effective contribution to the signal is $I_{\text{eff}}^2/2$. Thus, the effective carrier density is given by

$$N_{\text{eff}}(t) \simeq \frac{1}{2}\left(\frac{\beta_2}{2\hbar\omega}\right)\int_{-\infty}^{t} I_{\text{eff}}^2\, dt'.$$

The resulting nonlinear polarization source term P_{NL} is proportional to E_bN_{eff}. In the case where E_b is not temporally overlapped with E_p or E_f, I_{eff}^2 becomes $2(E_fE_p^* + \text{c.c.})|E_f|^2$ (effects of grating decay will be treated in the next section). Assuming phase distortions on E_p to be small, $E_p^* = E_{p0}\exp\{+ik_p(z\cos\theta + x\sin\theta)\}$ and $E_f = E_{f0}\exp\{-ik_fz\}$, so that N_{eff} can be written as

$$N_{\text{eff}}(t) = \left(\frac{\beta_2}{2\hbar\omega}\right)\left(\frac{nc\epsilon_0}{2}\right)^2 \cdot 2\cos[K_gx]\int_{-\infty}^{t}|E_f(t')|^3|E_p(t')|\, dt' \quad (7)$$

where $\boldsymbol{K}_g = \boldsymbol{k}_f - \boldsymbol{k}_p$ is the grating wave vector. In the limit of small θ, $K_g \simeq 2\pi\theta/\lambda$, where λ is the free-space wavelength. Since $E_c \propto P_{\text{NL}}$, the total irradiance dependence of the DFWM signal is

$$I_c \propto I_bI_pI_f^3. \quad (8)$$

In order to verify this, we measured the DFWM signal in CdTe at 1.064 μm as a function of I_f, only with the backward pump delayed by 240 ps. The signal was plotted logarithmically against I_f and the slope of the resulting straight line was found to be 2.8 ± 0.3 in accordance with (8).

A similar expression can be obtained when the carriers are generated via a three-photon absorption process. Following an analogous procedure, the end result is a seventh order dependence of the DFWM signal on the input beams as three-photon absorption is an Im $\chi^{(5)}$ process. In our experiments in ZnSe at 1.064 μm, we find that at higher input irradiances, on the order of 1.2 GW/cm^2 per strong pump, a free-carrier tail became evident. Fig. 6 shows a log-log plot of the irradiance dependence for $\tau_b = 240$ ps. A best fit gives a dependence of $I^{6.9\pm0.2}$, agreeing closely with the power of 7 expected for 3PA induced carrier refraction. Under our experimental conditions with the backward pump delayed, the DFWM signal dependence is

$$I_c \propto I_bI_pI_f^5. \quad (9)$$

Fig. 7 shows a similar plot to Fig. 6, except that in this case only I_f is varied resulting in a power dependence of $I^{5.1\pm0.3}$, close to the power of 5 predicted in (9).

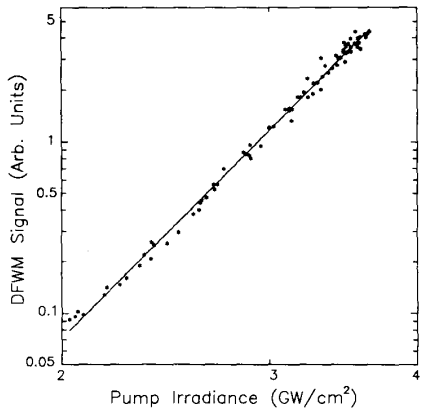

Fig. 6. Logarithmic plot of the DFWM signal resulting from the three-photon absorption generated carrier grating in ZnSe at 1.064 μm versus the total input irradiance. The measurement was performed with the backward pump delayed by 240 ps. The solid line is a best fit to the data, indicating an $I^{6.9\pm0.2}$ dependence.

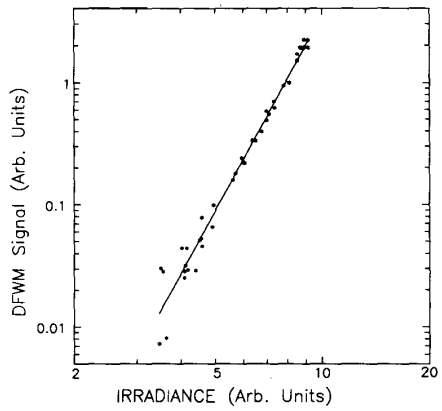

Fig. 7. As Fig. 6, but with only the forward pump varied and the backward pump and probe held at constant irradiance. The forward pump energy was not calibrated for this experiment. The solid line is the best fit, giving an $I_f^{5.1\pm0.3}$ dependence for the DFWM signal in this case.

D. Temporal Evolution of Diffraction Efficiency in ZnSe

In order to determine the refractive index change per excited carrier pair per unit volume, σ_n (units of cm^3), we need to measure the diffraction efficiency of the carrier grating in the absence of the third order signal. This necessitates measurement of the DFWM signal at a delay long compared to the pulsewidth. σ_n is thus obtained by fitting the theoretical diffraction efficiency to the measured value. However, to calculate this diffraction efficiency we require a knowledge of the temporal dependence of the density of 2PA-generated carriers $N(x, t)$. This is governed by [15]

$$\frac{dN_{\text{eff}}(x,t)}{dt} + \frac{N_{\text{eff}}(x,t)}{\tau} - D\frac{d^2N_{\text{eff}}(x,t)}{dx^2} = \frac{\beta I_{\text{eff}}^2(x,t)}{2\hbar\omega} \quad (10)$$

where τ is the carrier decay time and D is the carrier diffusion coefficient. We use a constant carrier lifetime as the carrier densities in our experiments are several orders of magnitude too low to have significant bimolecular or Auger recombination. This is verified by the I^5 power dependence in our experiments. Since the beam radius is much larger than the grating period we assume the diffusion occurs only in the direction x between grating maxima and minima. Further, we have assumed low excitation such that the spatial amplitude of I^2 does not vary in the propagation direction z, i.e., $\beta IL \ll 1$ which was true for the irradiance levels used. The solution to the diffusion equation is then

$$N_{\text{eff}}(x, t) = \frac{\beta_2}{2\hbar\omega} \exp(-t/\tau_g) \cdot \int_{-\infty}^{t} \exp(t'/\tau_g) I_{\text{eff}}^2(x, y, t')\, dt' \quad (11)$$

where τ_g is the total decay time of the grating, given by $\tau_g = \tau_D\tau_R/(\tau_D + \tau_R)$. Here τ_D is the grating diffusion lifetime and τ_R is the carrier recombination lifetime [14]. We have again assumed that E_b is time delayed. Note that the product $E_f E_p^*$ in I_{eff}^2 has a term $2|E_f\|E_p| \exp(iK_g x)$, where $K_g = 2\pi/\Lambda$, and $\Lambda = \lambda/[2n \sin(\theta/2)]$ is the grating spacing. Hence $1/\tau_g = (4\pi^2 D)/\Lambda^2 + 1/\tau$ [16]. For the sample thickness and grating spacings used, we were always in the thick grating limit. The diffraction efficiency for weak excitation of a thick lossless phase grating was derived by Kogelnik [4], [17] to be

$$\eta = \sin^2\left(\frac{\Delta n \pi L}{\lambda \cos\theta}\right) \simeq \left(\frac{\Delta n \pi L}{\lambda \cos\theta}\right)^2 \quad (12)$$

where $\Delta n = \sigma_n N_{\text{eff}}$. The energy diffracted into the conjugate beam ϵ_c is then given by temporally and spatially integrating the product of the diffraction efficiency η and the beam irradiance incident on the grating giving

$$\epsilon_c(\tau_b) = \int_{-\infty}^{\infty} \eta(x', y', t') I_b(x', y', t' - \tau_b)\, dx'\, dy'\, dt' \quad (13)$$

where $I_b(x, y, t) = I_{b0} \exp[-(x^2 + y^2)/w^2 - (t^2/t_p)^2]$. Here τ_b accounts for the time delay of the backward pump with respect to the interfering beams. Note for $\eta = 1$, (13) gives the energy in the backward pump ϵ_b. Defining η_ϵ as the energy diffraction efficiency, we find

$$\eta_\epsilon = \epsilon_c/\epsilon_b = \xi(1 + \xi)^2 \frac{2\sqrt{2}\beta_2^2\sigma_n^2 I_f^4 \sqrt{\pi} t_p L^2}{80 (\hbar\omega)^2 \lambda^2 \cos^2\theta} \exp(t_p^2/4\tau_g^2) \cdot \int_{-\infty}^{\infty} \exp(-(t' - \tau_b)^2/t_p^2) \exp(-2t'/\tau_g) \cdot \{1 + \text{erf}[\sqrt{2}/t_p(t' - t_p^2/4\tau_g)]\}^2\, dt' \quad (14)$$

where ξ is the ratio of I_p to I_f. Note that this derivation is valid only when the beam widths are large compared to the grating period, when the length of interaction of the interfering beams is much larger than the sample thickness, and when absorption of the interacting beams is small. Given $\beta_2 = 5.5$ cm/GW [10] at 532 nm for ZnSe, a numerical fit of (14) yields σ_n and τ_g.

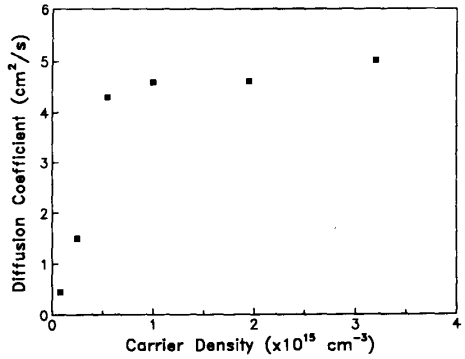

Fig. 8. Plot of measured diffusion coefficient versus peak carrier density.

The experimentally measured value for the diffraction efficiency for ZnSe at 0.532 μm at $\tau = 240$ ps is $\eta = 6.8 \times 10^{-5}$ for a pump-probe angle θ of 13°. The grating decay rate τ_g was determined from the best fit exponential decay to the data at long delays for several input irradiances. Using $t_p = 18$ ps (HW1/eM in irradiance), and $\tau_g = 247$ ps, and numerically integrating (14), we obtain $|\sigma_n| \simeq 5.1 \pm 2.5 \times 10^{-21}$ cm^3. This is considerably larger than the result of another recent measurement of σ_n that obtained $\sigma_n = -0.8 \pm 0.2 \times 10^{-21}$ [18] and probably indicates the difficulty of obtaining accurate absolute values of nonlinearities from multiple beam diffraction efficiency measurements. Note that the measurement in [18] showed the sign of σ_n to be negative [3]. The uncertainties stated are relative fitting errors. The absolute error bars on σ_n are estimated to be $\simeq 50\%$.

We were also able to extract the density dependence of the carrier diffusion coefficient by measuring the angular dependence of the grating decay time for a number of different pump irradiances and therefore different carrier densities [19]. This dependence is plotted in Fig. 8. We find that for irradiances above 40 MW/cm^2, corresponding to carrier densities $>5 \times 10^{14}$ cm^{-3}, D maintains a constant value of 4.5 ± 0.5 cm^2/s, while below 5×10^{14} cm^{-3}, the diffusion coefficient decreases rapidly. For these densities we do not expect to have any density dependence of either the mobility or the recombination lifetime. We therefore propose that the small diffusion coefficient at low density may be due to trapping of the 2PA excited carriers. As the carrier density is increased, these traps become filled and the diffusion is dominated by the ambipolar mobility. This high density result is comparable to the result of 2.5 ± 0.5 cm^2/s obtained by Jarasiunas and Gerritsen, but their carrier density is not given [3]. Using data from Hall mobility measurements in ZnSe, [20] we calculate an ambipolar mobility of 26 cm^2 V^{-1} s^{-1}, corresponding to a diffusion coefficient of 0.7 cm^2/s at 300°K. This is in good agreement with our low density measurements, since the Hall mobility measurements are

performed with low dopant densities. It should be noted that over the entire range of carrier densities measured, the carrier nonlinearity is fifth order. This rules out the possibility that the traps are filled by linear absorption. These measurements also gave an estimate for the recombination lifetime of $\tau_R = 725 \pm 275$ ps.

IV. Conclusion

We have presented a series of picosecond transient DFWM measurements performed in two direct-gap II–VI semiconductors. For ZnSe, large third order nonlinear mechanisms were observed both at 0.532 and 1.064 μm. The origin of these fast third order nonlinearities is believed to be due to both two-photon absorption and the bound electronic Kerr effect [8]. The magnitude of the nonlinear susceptibilities found were $|\chi^{(3)}| \simeq 1.9 \pm 0.57 \times 10^{-11}$ esu and $1.2 \pm 0.35 \times 10^{-11}$ esu at 0.532 μm and 1.064 μm, respectively. Similarly, for CdTe a third order effect yielded a $|\chi^{(3)}| \simeq 7.2 \pm 2.1 \times 10^{-10}$ esu at 1.064 μm. Combined with independent measurements [10] of the two-photon absorption coefficients in these materials, this indicates that the measured susceptibility in ZnSe at 532 nm and CdTe at 1.06 μm is dominated by nonlinear refraction. As there is no 2PA in ZnSe at 1.06 μm, we conclude that this susceptibility is entirely refractive. Other data [8] indicates that in ZnSe n_2 is negative at 0.532 μm and positive at 1.064 μm, while in CdTe at 1.064 μm, n_2 is negative. Higher order nonlinearities (higher than third order) were also observed in both semiconductors. These nonlinearities are attributed to nonlinear absorption induced carrier refraction.

When carriers are excited via the absorption of two photons, we have seen a fifth order dependence of the conjugate field on the input fields as expected. In the same manner, for carrier excitation achieved via the absorption of three photons, an effective seventh order nonlinearity was found.

For ZnSe at 0.532 μm and for low excitation, a value for the index of refraction per carrier pair generated of $\sigma_n \simeq 5.1 \pm 2.5 \times 10^{-21}$ cm^3 was estimated. By monitoring the grating decay times for different grating spacings, the density dependence of the diffusion coefficient was extracted.

Acknowledgment

We wish to thank B. S. Wherrett for his critical review of this paper, G. M. Moharam for useful discussions on the diffraction efficiency calculations, and E. Miesak for help in taking data.

References

[1] M. Sheik-Bahae, A. A. Said, T. H. Wei, D. J. Hagan, and E. W. Van Stryland, "Sensitive measurement of optical nonlinearities using a single beam," *IEEE J. Quantum Electron.*, vol. 26, pp. 760–769, 1990.

[2] R. K. Jain and M. B. Klein, "Degenerate four-wave mixing in semiconductors," in *Optical Phase Conjugation*, R. A. Fisher, Ed. New York: Academic, 1983, pp. 307–415.

[3] K. Jarasiunas and H. J. Gerritsen, "Ambipolar diffusion measurements in semiconductors using nonlinear transient gratings," *Appl. Phys. Lett.*, vol. 33, pp. 190–193, 1978.

[4] H. Kogelnik, "Coupled wave theory for thick hologram gratings," *Bell Syst. Tech. J.*, vol. 48, pp. 2909–2947, 1969.

[5] Sample obtained from II–VI, Inc., Saxonburg, PA.

[6] E. W. Van Stryland, Y. Y. Wu, D. J. Hagan, M. J. Soileau, and K. Mansour, "Optical limiting with semiconductors," *J. Opt. Soc. Amer. B.*, vol. 5, pp. 1980–1989, 1988.

[7] J. J. Wynne, "Optical third-order mixing in GaAs, Ge, Si, and InAs," *Phys. Rev.*, vol. 178, pp. 1295–1303, 1969.

[8] M. Sheik-Bahae, D. J. Hagan, and E. W. Van Stryland, "Dispersion and band-gap scaling of the electronic Kerr effect in solids associated with two-photon absorption," *Phys. Rev. Lett.*, vol. 65, pp. 96–99, 1989.

[9] Landolt–Börnstein, *Numerical Data and Functional Relationships in Science and Technology*, Volume 17, Semiconductors, K.-H. Hellewege, Ed. New York: Springer-Verlag, 1982.

[10] E. W. Van Stryland, H. Vanherzeele, M. A. Woodall, M. J. Soileau, A. L. Smirl, S. Guha, T. F. Boggess, "Two-photon absorption, nonlinear refraction and optical limiting in semiconductors," *Opt. Eng.*, vol. 24, pp. 613–623, 1985.

[11] P. N. Butcher, "Nonlinear optical phenomena," *Bulletin 200*, Ohio State Univ., Columbus, OH, 1965.

[12] M. J. Soileau, W. E. Williams, and E. W. Van Stryland, "Optical power limiter with picosecond response time," *IEEE J. Quantum Electron.*, vol. QE-19, p. 731, 1983.

[13] R. Adair, L. L. Chase, and S. A. Payne, "Nonlinear refractive index of optical crystals," *Phys. Rev. B*, vol. 39, pp. 3377–3350, 1987.

[14] J. H. Bechtel and W. L. Smith, "Two-photon absorption in semiconductors with picosecond laser pulses," *Phys. Rev. B*, vol. 13, pp. 3515–3522, 1976.

[15] W. Van Roosbroeck, "The transport of added current carriers in a homogeneous semiconductor," *Phys. Rev.*, vol. 91, pp. 282–289, 1953.

[16] J. R. Salcedo, A. E. Siegman, D. D. Dlott, and M. D. Fayer, "Dynamics of energy transport in molecular crystals: the picosecond transient grating method," *Phys. Rev. Lett.*, vol. 41, p. 131, 1978.

[17] H. J. Eichler, P. Gunter, and D. W. Pohl, *Laser-Induced Dynamic Gratings*, Springer Series in Optical Sciences, J. M. Enoch, D. L. MacAdam, A. L. Schawlow, K. Shimoda, and T. Tamir, Eds. New York: Springer-Verlag, 1988.

[18] A. A. Said, M. Sheik-Bahae, D. J. Hagan, E. J. Canto-Said, Y. Y. Wu, J. Young, T. H. Wei, and E. W. Van Stryland, "Nonlinearities in semiconductors for optical limiting," in *Proc. SPIE*, Electro-Optical Materials for Switches, Coatings, Sensor Optics, and Detectors, Orlando, 1990, conf. 1370.

[19] D. J. Hagan, H. A. MacKenzie, H. A. Al Attar, and W. J. Firth, "Carrier diffusion measurements in InSb by the angular dependence of degenerate four-wave mixing," *Opt. Lett.*, vol. 10, p. 187, 1985.

[20] B. Ray, *II–VI compounds*. Edinburgh: Pergamon, 1969, ch.6.

E. J. Canto-Said, photograph and biography not available at the time of publication.

D. J. Hagan (M'87), for a photograph and biography, see p. 1309 of the June 1991 issue of this JOURNAL.

J. Young, photograph and biography not available at the time of publication.

Eric W. Van Stryland (M'84–SM'90), for a photograph and biography, see p. 1309 of the June 1991 issue of this JOURNAL.